THE JOURNAL OF PHYSICAL CHEMISTRY A LETTERS

2009, *113,* 13443–13447
Published on Web 11/03/2009

Distinctive IR Signature of $CO_3^{\bullet-}$ and CO_3^{2-} Hydrated Clusters: A Theoretical Study

A. K. Pathak[†] and D. K. Maity*[,‡]

Radiation and Photochemistry Division and Theoretical Chemistry Section, Chemistry Group, Bhabha Atomic Research Centre, Mumbai 400085, India

Received: August 6, 2009; Revised Manuscript Received: October 29, 2009

Weighted average IR spectra of $CO_3^{\bullet-}\cdot nH_2O$ ($n = 1-6$) clusters are reported and compared with those of $CO_3^{2-}\cdot nH_2O$ ($n = 1-6$) clusters based on quantum chemical calculations. Simulated annealing combined with the Monte Carlo sampling method is also applied to locate the global minimum energy structure. It is observed that hydrated clusters of $CO_3^{\bullet-}$ ion having cyclic water networks are the most stable structure in each size of hydrated cluster. IR bands at the lower side of the O−H stretching region of water correspond to single/double hydrogen bonding interaction, and those in the higher side correspond to inter water hydrogen bonding for the lower clusters ($n = 2-3$). For the tetrahydrated cluster of $CO_3^{\bullet-}$ ion, a complete crossover of the IR spectra in the O−H stretching region occurred. Cyclic water networks having three or four solvent water molecules are characterized by strong peaks at 3550 and 3450 cm^{-1}. In the case of $CO_3^{\bullet-}\cdot nH_2O$ clusters, O−H stretching bands of all of the solvent water molecules are above 3100 cm^{-1} in contrast to that of $CO_3^{2-}\cdot nH_2O$ clusters showing distinctive IR signature. This suggests that size selected hydrated clusters of $CO_3^{\bullet-}$ and CO_3^{2-} ions can easily be distinguished on the basis of their IR spectra.

1. Introduction

Theoretical analysis of IR bands in the O−H stretching region of water in a hydrated cluster of small anionic solute is shown to depict a comprehensible picture on the deformation pattern of hydrogen bonded networks of solvent water molecules.[1,2] Of late, IR spectra of size selected clusters are effectively applied to understand the structure and growth motif of solvent water molecules around various charged solutes in the process of microhydration. In this context, mostly spherical halide anions (F^-, Cl^-, Br^-, and I^-) are studied.[2−4] Microhydration of diatomic and polyatomic species like O_2^-, OH^-, $Cl_2^{\bullet-}$, $Br_2^{\bullet-}$, NO_3^-, etc., is also well studied.[1,2,5−9] On the basis of these studies, it is understood that these water clusters are stabilized by single hydrogen bonding (SHB), double hydrogen bonding (DHB), and inter water hydrogen bonding (WHB) networks. Water molecules form a cyclic network in the hydration shell to stabilize hydrated clusters.

Hydroxyl radical ($^{\bullet}OH$) reacts with CO_3^{2-} or HCO_3^- anions to form a transient species which has a broad and moderately strong absorption ($\varepsilon \sim 1980\ M^{-1}\ cm^{-1}$) in the visible region with an absorption maximum, λ_{max}, at ∼600 nm. This absorption maximum is assigned to the carbonate radical anion, $CO_3^{\bullet-}$, a specific one electron oxidizing species. This radical anion has been the subject of extensive research not only due to its role as a terminal ion in atmospheric chemistry but also due to its rich and various photophysical properties. Oxidative chemistry of carbonate radical anion, $CO_3^{\bullet-}$, has been studied due to its vital function in inflammatory processes of biological systems.[10] It is also reported that carbonate radical anion is produced in the physiological system during xanthine oxidase turnover; xanthine oxidase is normally recognized as the key enzyme in purine catabolism.[11] Thermochemical properties of carbonate radical anion and the reduction potential value of the $CO_3^{2-}/CO_3^{\bullet-}$ redox couple are reported on the basis of first principle based electronic structure calculations.[12] Attempts are also made to study the structure and energetics of a small size ($n \leq 6$) hydrated cluster of singly negative charged carbonate radical ion, $CO_3^{\bullet-}$, with an attempt to extract the bulk detachment energy of $CO_3^{\bullet-}$(aq) from its finite size hydrated clusters.[13,14] Structure and vibrational properties are reported for doubly negative charged carbonate hydrated clusters, $CO_3^{2-}\cdot nH_2O$ of size $n = 1-6$.[15] This doubly negative charged anion, CO_3^{2-}, is one of the precursors of carbonate radical anion, $CO_3^{\bullet-}$, and both of them have D_{3h} symmetry. Both of the species are part of carbonate chemistry and can exist together in nature; they are also detected in atmospheric water droplets. As the two species differ in their charge, they are expected to interact differently with water molecules and to follow different hydration growth routes to form bulk aqueous anion, CO_3^{2-}(aq) or $CO_3^{\bullet-}$(aq). As a result, it is also expected to see different features in IR spectra of the size selected hydrated clusters of these two carbonate anions. Is there any IR signature to distinguish these two anions in their water embedded clusters? It will be interesting to see whether by critical analysis of IR spectra in the O−H stretching region of solvent water molecules one can distinguish between $CO_3^{\bullet-}$−water and CO_3^{2-}−water clusters. In this Letter, we report weighted average IR spectra of $CO_3^{\bullet-}\cdot nH_2O$ ($n = 1-6$) clusters applying density functional theory and compare the results to those of $CO_3^{2-}\cdot nH_2O$ clusters to identify distinctive IR signature.

* To whom correspondence should be addressed. E-mail: dkmaity@barc.gov.in.
[†] Radiation and Photochemistry Division.
[‡] Theoretical Chemistry Section.

10.1021/jp907577j CCC: $40.75

2. Theoretical Methods

Geometry optimizations of $CO_3^{\bullet-}\cdot nH_2O$ and $CO_3^{2-}\cdot nH_2O$ clusters are carried out following the popular hybrid density functional, namely, Becke's three parameter nonlocal exchange (B3) and Lee−Yang−Parr (LYP) nonlocal correlation functionals (B3LYP) with the triple split valence 6-311++G(d,p) set of basis function. The pseudo Newton−Raphson (NR) based algorithm is applied to carry out a geometry search in each case with various initial structures designed systematically following a bottom-up approach to find out all possible minimum energy structrures.[8] Simulated annealing combined with the Monte Carlo sampling method is applied to locate the global minimum energy structure in each case and to verify the predicted most stable structure following the NR procedure.[16,17] Random structures are generated by carrying out Monte Carlo steps at a temperature range of 2000 to 100 K for more than 8000 steps. Vibrational analysis is performed for all of the optimized structures to check the nature of the equilibrium geometry and to generate IR spectra. As a large number of equilibrium structures are predicted for a particular size of cluster, weighted average IR spectra are generated. In principle, it should be best compared to the experimental spectra, as under the experimental condition all of the stable equilibrium structures are expected to have a contribution to the IR spectra along with the global minimum energy structure. Population (P_i) of the ith equilibrium structure of each size clusters is calculated on the basis of free energy change (ΔG_i) at temperature T following Boltzmann distribution, i.e., $P_i = \exp(-\Delta G_i/kT)$. Note that ΔG_i values are calculated by assuming the normal modes of the cluster as independent harmonic oscillators. Cluster experiments (NVE ensemble) are usually carried out at low temperature, and the temperature is often not known precisely. At present, weighted average IR spectra are calculated at $T = 150$ K, an average experimental temperature at which these hydrated clusters are expected to be stable. The weighted average IR spectra have been constructed applying the relation $IR^{wt} = \sum_i P_i IR_i$. IR spectra are generated from a list of vibrational frequencies and intensities using Lorentzian band shape and half-width of 10 cm^{-1} for each of the $3N - 6$ vibration modes calculated. Vibrational analysis with anharmonic corrections using the vibrational self-consistent field (VSCF) method is also carried out.[18] All of the electronic structure calculations are carried out applying the GAMESS program system.[19]

3. Results and Discussion

To choose a DFT functional suitable for these systems, several pure and hybrid correlated density functionals are considered for mono- and dihydrated clusters of both of the ions to find equilibrium structures. The calculated geometrical parameters are compared with those of MP2 results, adopting the same set of basis functions, 6-311++G(d,p). It is observed that the hybrid B3LYP functional produces the best results compared to MP2 and thus the B3LYP functional is applied for the rest. Various possible initial structures of $CO_3^{\bullet-}\cdot nH_2O$ and $CO_3^{-2}\cdot nH_2O$ clusters ($n = 1-6$) are considered for geometry optimization, and a number of minimum energy equilibrium structures are obtained. Simulated annealing combined with the Monte Carlo sampling algorithm is also applied to check if the global minimum energy structure is included in each case. It is observed that the present bottom-up approach adopted for designing the initial structures followed by full geometry optimization does not miss the global minimum structure in the case of $CO_3^{\bullet-}\cdot nH_2O$ and $CO_3^{-2}\cdot nH_2O$ clusters ($n = 1-6$).

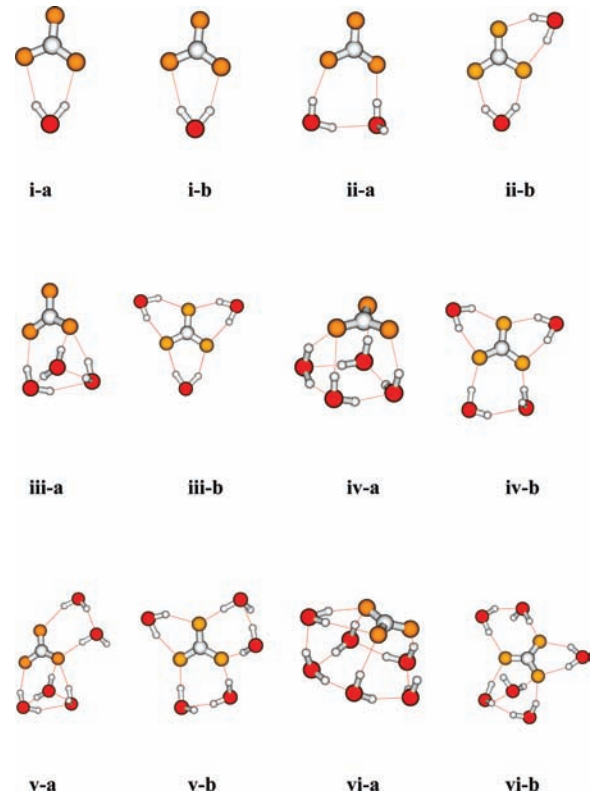

Figure 1. Fully optimized global minimum energy structure of (i-a) $CO_3^{\bullet-}\cdot H_2O$, (i-b) $CO_3^{2-}\cdot H_2O$, (ii-a) $CO_3^{\bullet-}\cdot 2H_2O$, (ii-b) $CO_3^{2-}\cdot 2H_2O$ (iii-a) $CO_3^{\bullet-}\cdot 3H_2O$, (iii-b) $CO_3^{2-}\cdot 3H_2O$ (iv-a) $CO_3^{\bullet-}\cdot 4H_2O$, (iv-b) $CO_3^{2-}\cdot 4H_2O$, (v-a) $CO_3^{\bullet-}\cdot 5H_2O$, (v-b) $CO_3^{2-}\cdot 5H_2O$, (vi-a) $CO_3^{\bullet-}\cdot 6H_2O$, and (vi-b) $CO_3^{2-}\cdot 6H_2O$. C atoms are shown by the gray color spheres; the smallest spheres refer to H atoms and the rest correspond to O atoms in each case. Yellow color spheres refer to the carbonate O atoms, and the rest (red in color) are water O atoms.

TABLE 1: Scaled O−H Stretching Frequency Span of Each Size of Clusters of $CO_3^{\bullet-}\cdot nH_2O$ and $CO_3^{2-}\cdot nH_2O$ ($n = 1-6$) at the B3LYP/6-311++G(d,p) Level of Theory[a]

	scaled O−H frequency range (cm^{-1})	
system[b]	$CO_3^{2-}\cdot nH_2O$	$CO_3^{\bullet-}\cdot nH_2O$
$n = 1$ (1, 1)	2902−3203	3458−3643
$n = 2$ (2, 3)	3000−3377	3235−3697
$n = 3$ (4, 4)	2530−3654	3272−3731
$n = 4$ (4, 4)	2258−3691	3284−3747
$n = 5$ (5, 4)	2433−3718	3344−3747
$n = 6$ (7, 5)	2548−3744	3293−3749

[a] The scaling factor is taken as 0.96 to account for the anharmonic nature of vibrations. [b] Values in parentheses are the number of minimum energy structures predicted for each size of clusters of $CO_3^{2-}\cdot nH_2O$ and $CO_3^{\bullet-}\cdot nH_2O$, respectively.

For $n = 1$, one stable minimum energy structure is obtained from two initial guess structures for both of the clusters and they are similar in structure, as displayed in Figure 1(ia-ib). The number of minimum energy structures predicted for each size cluster of $CO_3^{\bullet-}\cdot nH_2O$ and $CO_3^{-2}\cdot nH_2O$ is mentioned in Table 1. In each case, initial guess structures designed on the basis of a bottom-up approach are much higher, but a few initial structures converge to the same minimum energy structure. The global minimum energy structure predicted for each size hydrated cluster of $CO_3^{\bullet-}\cdot nH_2O$ and $CO_3^{-2}\cdot nH_2O$ ($n = 1-6$) is displayed in Figure 1. These most stable structures are predicted on the basis of the internal energy of the clusters. In the case of a few clusters, a different structure is predicted as

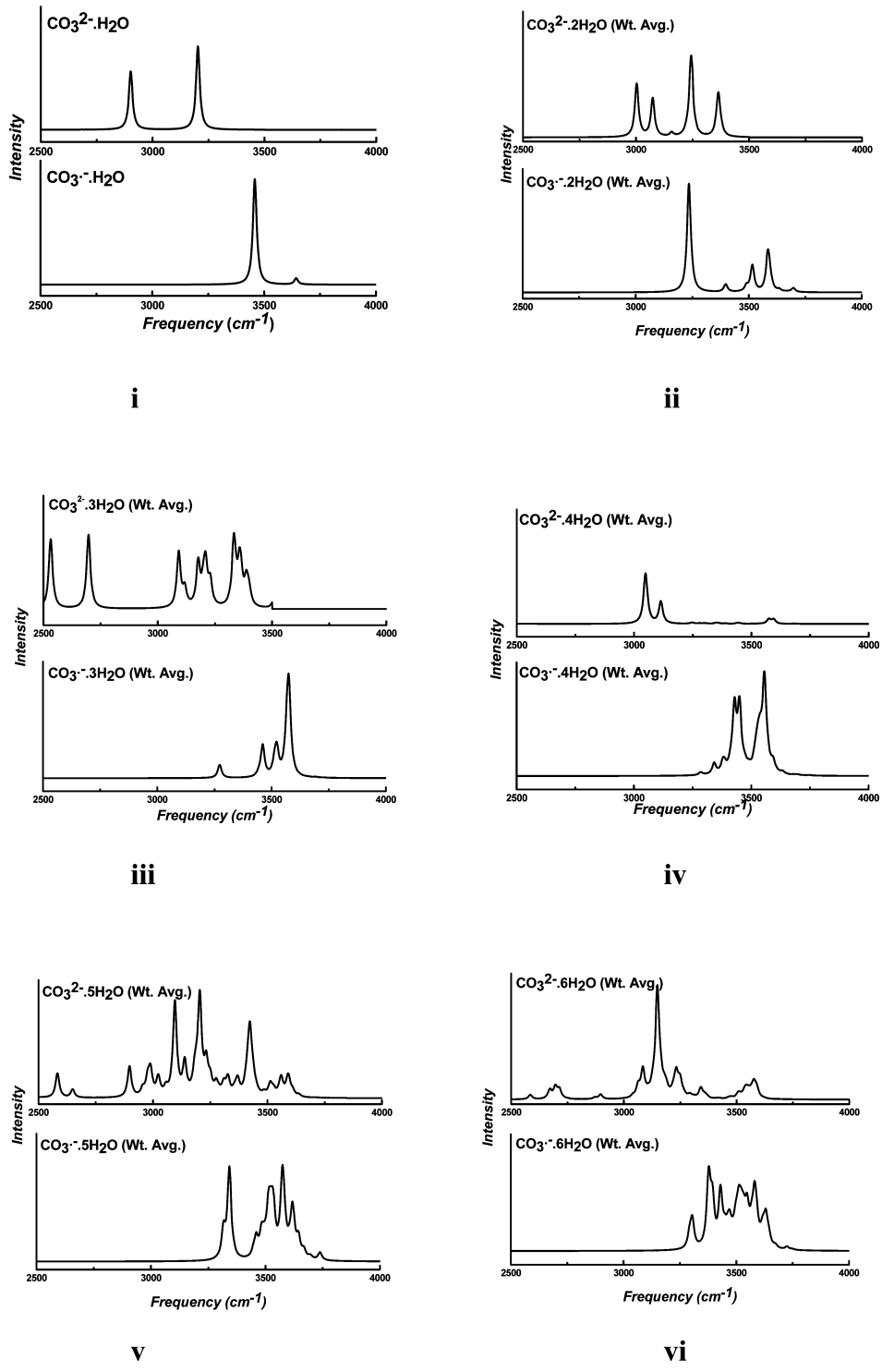

Figure 2. Calculated scaled weighted average IR spectra for the hydrated clusters of CO_3^{2-} and $CO_3^{\bullet-}$ ions: (i) $n = 1$; (ii) $n = 2$; (iii) $n = 3$; (iv) $n = 4$; (v) $n = 5$; (vi) $n = 6$. The weight factor of each equilibrium structure is calculated on the basis of free energy change (ΔG_i) at 150 K following Boltzmann distribution. Lorentzian line shape is considered with a peak half-width of 10 cm^{-1} for all of the IR plots. The scaling factor is taken as 0.96 to account for the anharmonic nature of vibrations.

the most stable one on the free energy landscape. It is observed that, for both of the anions, hydrated clusters are stabilized by double hydrogen bonding (DHB), single hydrogen bonding (SHB), and inter water hydrogen bonding (WHB). In the case of DHB, both of the H atoms from a solvent water molecule form an ionic H-bond with any two O atoms of the solute. In the case of SHB, only one H atom of a solvent water molecule forms an ionic H-bond with any one O atom of the solute. Hydrogen bonded water networks having two, three, four, or five solvent H_2O units are present in these clusters. It is observed that a hydrated cluster having cyclic water networks is the most stable minimum energy structure in the case of the $CO_3^{\bullet-}$ system. However, in the case of the $CO_3^{2-}\cdot nH_2O$ system for $n = 1-5$, the structure having cyclic water network units is less stable compared to the structures in which solvent water molecules are directly connected to the ion through SHB/DHB. The calculated average energy for SHB and WHB interactions is 81.6 and 25.1 kJ/mol, respectively, in the case of CO_3^{2-}

hydrated clusters. However, the same for $CO_3^{\bullet-}$ hydrated clusters is 35.5 and 25.1 kJ/mol, respectively.

As discussed in the previous sections, $CO_3^{\bullet-}\cdot nH_2O$ and $CO_3^{2-}\cdot nH_2O$ clusters are stabilized by the interaction between O (of $CO_3^{\bullet-}/CO_3^{2-}$) and H (from H_2O) atoms as well as inter water H-bonding interaction. Due to these interactions, it is expected that bands due to stretching (O−H) and bending modes of H_2O in the hydrated clusters get shifted compared to that of a free water molecule. IR spectra for all of the conformers of both of the clusters are calculated. Figure 2 depicts the weighted average IR spectra of the hydrated clusters of size $n \leq 6$. Lorentzian line shape is considered with a peak half-width of 10 cm^{-1} for all of the IR spectra plots. On the basis of free water molecule vibration, the scaling factor is taken as 0.96 to account for the anharmonic nature of vibration; all of the bonds are not affected equally by the anharmonic nature of vibrations, though. It is to be noted that anharmonic calculations using the VSCF method for the small size clusters ($n = 1-2$) yields a different scaling factor for different modes. However, anharmonic calculation is very expensive and it is difficult to scale an individual mode for the higher clusters. Thus, we use a uniform scaling factor of 0.96 throughout the study. Calculated vibrational frequencies for free water are 1531, 3663, and 3756 cm^{-1}, respectively, for bending (ν_{bend}), symmetrical stretching (ν_{sym}), and asymmetrical stretching (ν_{asym}) at the B3LYP/6-311++G(d,p) level of theory. The scaled IR spectra of $CO_3^{\bullet-}$ have three bands at 360, 800, and 1220 cm^{-1} and are assigned to in-plane bending, out-of-plane bending, and asymmetric C−O stretching modes, respectively. The symmetric C−O stretching mode is calculated to be too weak to detect. On the other hand, scaled IR spectra of CO_3^{2-} have a single sharp band at 1260 cm^{-1} and are assigned to C═O stretching. Other IR bands are too weak to observe.

The weighted average scaled IR spectra of $CO_3^{2-}\cdot nH_2O$ clusters ($n = 1-6$) are shown in Figure 2(i-vi). The calculated range of scaled harmonic frequency for O−H stretching is supplied in Table 1 for both of the systems. The IR spectra of each cluster are characterized by a large shift of the O−H stretching mode compared to that of the free water mode, and at least one peak for all of the clusters in the O−H stretching region is predicted below 3100 cm^{-1} (see Table 1). It is observed that IR bands due to WHB interaction appear in the higher side of the O−H stretching region and the band due to SHB/DHB interaction appears in the lower side of the O−H stretching region in all of the cases. Red shifting of the O−H stretching band ($\Delta\nu$) is observed as large as 1500 cm^{-1} in these hydrated clusters compared to free water, as may be seen from Table 1.

The scaled IR spectra of the monohydrated cluster ($CO_3^{\bullet-}\cdot H_2O$) having a strong peak ~3460 cm^{-1} and a very weak peak ~3640 cm^{-1} in the O−H stretching region is shown in Figure 2-i. The weighted average IR spectra of the $CO_3^{\bullet-}\cdot 2H_2O$ (Figure 2-ii) cluster is complex and has multiple peaks in the O−H stretching region. The weighted average IR spectra of $CO_3^{\bullet-}\cdot 3H_2O$ is shown in Figure 2-iii, showing multiple peaks in the O−H stretching region. The peak at the lower side of the O−H stretching region corresponds to SHB/DHB interactions, and that at the higher side corresponds to WHB interactions. At $n = 4$, a complete crossover of the IR spectra in the O−H stretching region is observed. Bands due to the O−H stretching mode having WHB interactions appear in the lower side, and those due to SHB/DHB interactions appear in the higher side of the O−H stretching region. Weighted average IR spectra of $CO_3^{\bullet-}\cdot 4H_2O$ and $CO_3^{\bullet-}\cdot 5H_2O$ (Figures 2-iv and 2-v) are characterized by two well separated bands in the O−H stretching region. This is due to the fact that the strength of all of the SHB interactions in these clusters is nearly the same, so for WHB interactions. The weighted average IR spectra of $CO_3^{\bullet-}\cdot 6H_2O$ are shown in Figure 2-vi, having multiple and complex features in the O−H stretching region. This suggests that SHB and WHB interactions present in the cluster are of different strengths. It is of note that the O−H stretching mode due to dangling hydrogen appeared at ~3700 cm^{-1} and the cyclic water network having three and four water molecules is characterized by a strong peak at 3550 and 3450 cm^{-1}, respectively. It is noticed that IR bands due to bending of H_2O and the normal modes of $CO_3^{\bullet-}$ are not affected due to microhydration. This is also true for the hydrated clusters of CO_3^{2-} ion. It is now clear that all of the bands in the O−H stretching regions appeared above 3100 cm^{-1} for $CO_3^{\bullet-}\cdot nH_2O$ clusters in contrast to that in $CO_3^{2-}\cdot nH_2O$ clusters. Thus, water embedded clusters of $CO_3^{\bullet-}$ and CO_3^{2-} ions can easily be distinguished on the basis of their IR spectra. Hopefully, the present study will stimulate further work to validate this observation.

4. Conclusions

Several minimum energy structures of $CO_3^{\bullet-}\cdot nH_2O$ and $CO_3^{2-}\cdot nH_2O$ ($n = 1-6$) clusters are obtained applying the Newton−Raphson based optimization procedure. Simulated annealing combined with the Monte Carlo sampling method is also applied to locate the global minimum energy structure. It is observed that careful designing of initial structures does not miss the global minimum in any case. Weighted average IR spectra of all of the hydrated clusters of both of the ions are simulated on the basis of the relative population of predicted minimum energy structures following Boltzmann population analysis. It is observed that IR bands due to WHB interaction appear in the higher side of the O−H stretching region and the band due to SHB/DHB interaction appears in the lower side of the O−H stretching region in the case of $CO_3^{2-}\cdot nH_2O$ clusters. For the lower hydrated clusters of the $CO_3^{\bullet-}$ ion, IR bands at the lower side of the O−H stretching region correspond to SHB/DHB interactions and those in the higher side correspond to WHB interactions. In the case of the tetrahydrated cluster, a complete crossover occurred in the appearance of IR bands due to SHB/DHB and WHB interactions. However, no such crossover is observed in the IR spectra of $CO_3^{2-}\cdot nH_2O$ clusters. All of the O−H stretching modes appeared above 3100 cm^{-1} for the $CO_3^{\bullet-}\cdot nH_2O$ clusters in contrast to those of the $CO_3^{2-}\cdot nH_2O$ clusters. Very large shifts of bands (~1500 cm^{-1}) are observed in the case of CO_3^{2-} clusters in contrast to the maximum shift of 450 cm^{-1} in the case of $CO_3^{\bullet-}$ clusters. Size selected water embedded clusters of $CO_3^{\bullet-}$ and CO_3^{2-} ions can easily be distinguished on the basis of their IR spectra.

Acknowledgment. Sincere thanks are due to Computer Centre, BARC, for providing the ANUPAM parallel computational facility. We thank Dr. T. Mukherjee, Dr. S. K. Sarkar, and Dr. S. K. Ghosh for their constant encouragement during the course of this work.

Supporting Information Available: Structures and free energy differences (ΔG) in kJ mol^{-1} at 150 K for $CO_3^{2-}\cdot nH_2O$ and $CO_3^{\bullet-}\cdot nH_2O$ ($n = 1-6$) systems. This material is available free of charge via the Internet at http://pubs.acs.org.

References and Notes

(1) Weber, J. M.; Kelley, J. A.; Nielson, S. B.; Ayotte, P.; Johnson, M. A. *Science* **2000**, *287*, 2461.

(2) Robertson, W. H.; Diken, E. G.; Price, E. A.; Shin, J. W.; Johnson, M. A. *Science* **2003**, *299*, 1367.
(3) Ayotte, P. G.; Weddle, H.; Kim, J.; Johnson, M. A. *J. Am. Chem. Soc.* **1998**, *120*, 12361.
(4) Lee, H. M.; Kim, D.; Kim, K. S. *J. Chem. Phys.* **2002**, *116*, 5509.
(5) Xantheas, S. S. *J. Am. Chem. Soc.* **1995**, *117*, 10373.
(6) Masamura, M. *J. Chem. Phys.* **2002**, *117*, 5257.
(7) Price, E. A.; Hammeer, N. I.; Johnson, M. A. *J. Phys. Chem. A* **2004**, *108*, 3910.
(8) Pathak, A. K.; Mukherjee, T.; Maity, D. K. *J. Chem. Phys.* **2006**, *125*, 074309; **2007**, *127*, 044304.
(9) (a) Pathak, A. K.; Mukherjee, T.; Maity, D. K. *J. Phys. Chem. A* **2008**, *112*, 3399. (b) Goebbert, D. J.; Garand, E.; Wende, T.; Bergmann, R.; Meijer, G.; Asmis, K. R.; Neumark, D. M. *J. Phys. Chem. A* **2009**, *113*, 7584.
(10) Crean, C.; Uvaydov, Y.; Geacintov, N. E.; Shafirovich, V. *Nucleic Acids Res.* **2007**, *36*, 742.
(11) Bonini, M. G.; Miyamoto, S.; Di Mascio, P.; Augusto, O. *J. Biol. Chem.* **2004**, *279*, 51836.
(12) Armstrong, D. A.; Waltz, W. L.; Rauk, A. *Can. J. Chem.* **2006**, *84*, 1614.
(13) Cappa, C. D.; Elrod, M. J. *Phys. Chem. Chem. Phys.* **2001**, *23*, 2986.
(14) Pathak, A. K.; Mukherjee, T.; Maity, D. K. *ChemPhysChem* **2008**, *9*, 2259.
(15) Pathak, A. K.; Mukherjee, T.; Maity, D. K. *Synth. React. Inorg., Met.-Org., Nano-Met. Chem.* **2008**, *38*, 76.
(16) Day, P. N.; Pachter, R.; Gordon, M. S.; Merrill, G. N. *J. Chem. Phys.* **2000**, *12*, 2063.
(17) Wales, D. J.; Scheraga, H. A. *Science* **1999**, *285*, 1368.
(18) Chaban, G. M.; Jung, J. O.; Gerber, R. B. *J. Chem. Phys.* **1999**, *111*, 1823.
(19) Schmidt, M. W.; Baldridge, K. K.; Boatz, J. A.; Elbert, S. T.; Gordon, M. S.; Jensen, J. H.; Koseki, S.; Matsunaga, N.; Nguyen, K. A.; Su, S. J.; Windus, T. L.; Dupuis, M.; Montgomery, J. A. *J. Comput. Chem.* **1993**, *14*, 1347.

JP907577J